Numerical Heat Transfer, Part A, 37:249–270, 2000

1040–7782/00 $12.00 + .00

THE EFFECTS OF RADIATION ON NATURAL CONVECTION IN A RECTANGULAR ENCLOSURE DIVIDED BY TWO PARTITIONS

Cho Young Han and Seung Wook Baek
Department of Aerospace Engineering, Korea Advanced Institute of Science and Technology, Taejon 305-701, Korea

The phenomena of radiation-affected steady-laminar natural convection in a rectangular enclosure with two incomplete partitions are numerically examined under a large temperature difference. Pure convection, convection with surface radiation, and convection with surface/gas radiation are considered and compared. To examine the effects of two incomplete partitions on thermofluid dynamics behavior, they are assumed to be very thin and adiabatic. The finite-volume method (FVM) is used for solving the radiative transport equation, assuming that partitions are radiatively opaque. After validating the numerical procedures, the detailed radiation effects were sought. Based on the results of this study, it was found that the radiation played a significant role in developing the fluid dynamic and thermal distributions compared with cases without radiation. Once radiation was involved, the surface radiation was dominant over the gas radiation. The baffle configuration was also found to affect the results of radiation.

INTRODUCTION

The problem of natural convection in an enclosure is one of the interesting topics concerning thermal and mass transport processes involved in various types of engineering systems such as thermal insulation in buildings, unexpected hostile fire hazard, chip cooling in electronic or computer equipment, and thermal behavior in nuclear reactors. For the case of a simple enclosure without any partition or obstruction, many researchers have made numerous investigations [1–4] during the past few decades. A more complex enclosure with a partition was also adopted to study its concurring natural convection.

Nansteel and Greif [5] examined the thermofluid mechanical effects of a partition that was positioned at the center of an enclosure. Lin and Bejan [6] also performed a similar experimental work in a partially divided enclosure. An asymptotic analysis for the flow field was done as well for a very low Rayleigh number. However, in these experiments, water was used as a working fluid to emulate a high Rayleigh number under the very low temperature difference imposed. Hence, it was impossible to effectively simulate a fire phenomenon in a building for which a large temperature difference is incurred. Chang et al. [7] numerically examined a rectangular enclosure with two partitions with finite thickness centered at an adiabatic ceiling as well as floor, for which the working fluid was assumed to be a

Received 3 August 1999; accepted 1 October 1999.

Address correspondence to Professor Seung Wook Baek, Department of Aerospcace Engineering, Korea Advanced Institute of Science and Technology, 373-1 Kusong-dong, Yusong-ku, Taejon 305-701, Korea. E-mail: swbaek@sorak.kaist.ac.kr

NOMENCLATURE

C_p	specific heat at constant pressure, J/(kg · K)	κ_a	absorption coefficient, 1/m
		μ	viscosity, kg/(m · s)
Fr	Froude number $[= u_o/(gL)^{1/2}]$	ρ	density, kg/m^3
g	gravitational acceleration, m/s^2	σ	Stefan–Boltzmann constant, 5.67×10^{-8} W/(m^2 · K^4)
Gr	Grashof number $[= g\beta_o \rho_o^2 L^3 (T_H - T_C)/\mu_o^2$ where $\beta = 1/T$ for ideal gas]	σ_s	scattering coefficient, 1/m
		τ	optical thickness $[= \beta L]$
H	irradiation, W/m^2	ϕ	azimuthal angle, rad
I	radiation intensity, W/(m^2 · Sr)	Φ	scattering phase function, 1/Sr
k	thermal conductivity, W/(m · K)	ω	scattering albedo
L	height and width of enclosure	Ω	solid angle, Sr
$\hat{n}$	unit normal vector		
Nu	Nusselt number $[= q_w L/(k_o \delta T_o)]$	**Superscript**	
p	pressure, N/m^2		
Pl	Planck number $[= k_o/(4\sigma T_o^3 L)]$	C	conduction
Pr	Prandtl number $[C_{po}\mu_o/k_o]$	m	direction of radiation
q	local heat flux, W/m^2	R	radiation
$\vec{r}$	position vector	T	total quantity
Re	Reynolds number $[= \rho_o u_o L/\mu_o]$	*	dimensionless quantities
s	distance traveled by ray	$'$	incoming direction
S	source term	$\sim$	additional terms
T	temperature, K		
T_C, T_H	cooled and heated isothermal wall temperature, K	**Subscripts**	
T_o	reference temperature $[= (T_H + T_C)/2]$, K	0	reference quantities
		e, w, n, s	east, west, north, and south faces of a control volume
u_o	reference velocity $[= (gL\delta)^{1/2}]$		
u, v	velocity components in x and y directions, m/s	E, W, N, S	east, west, north, and south neighbors of the grid point P
x, y	Cartesian coordinates	L	left-hand side
β	extinction coefficient, 1/m	nb	neighbor
δ	overheat ratio $[= (T_H - T_C)/T_o]$	P	pertaining to the grid point P
ε	emissivity	R	right-hand side
θ	polar angle, rad	w	wall

participating medium under a large temperature difference. While adopting the radial flux method as a radiation solving method, they worked on a numerical manipulation of radiatively opaque obstructions in a computational domain. However, due to the technique used therein, an additional radial grid had to be introduced for a radiation solver, which is totally different from the usual grid configuration used for solving a flow field. Then Bajorek and Lloyd [8] carried out a limited experimentation to support the numerical results by Chang et al. [7].

In this study, different from the previous studies, natural convection induced by a large temperature difference is investigated in a rectangular enclosure in a more complex configuration. The two thin adiabatic partitions (one on the top and the other at the bottom) are oriented in skew rather than in line so that the surface radiation between them becomes more enhanced. The FVM [9] is utilized to solve the radiation transport adopting the same computational grid as used in solving the flow field, in which the adiabatic partitions are assumed to be radiatively opaque.

After discussing the numerical procedure adopted to handle the interaction of radiation with natural convection, the effects of two partitions on the thermofluid dynamics behavior in an enclosure with gas radiation effects are considered and discussed in detail.

THEORETICAL MODEL

A schematic of the enclosure with two partitions considered in this study is presented in Figure 1. In the square enclosure of height L and length L, one partition of length $0.6L$ is positioned at $x = 0.3L$ and the other at $x = 0.7L$, respectively. To examine the effects of the partition configurations on the natural convection as well as radiation, two different cases are considered. For case I, one partition is located on the left-hand side of the floor and the other on the right-hand side of the ceiling as shown in Figure 1*a*, whereas it is vice versa for case II as shown in Figure 1*b*. While the ceiling and floor are assumed to be insulated for both radiation and conduction, the left- and right-hand-side walls are

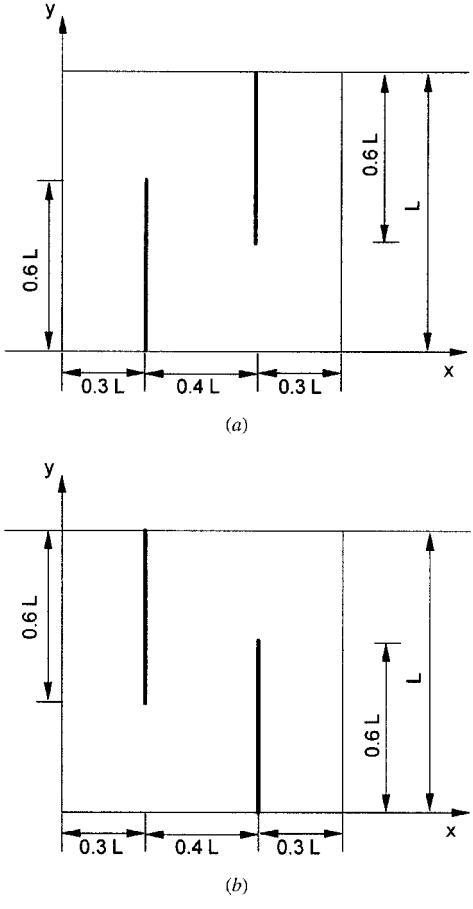

Figure 1. Schematics of the complex enclosures: (*a*) case I; (*b*) case II.

kept at T_H at $x = 0$ and T_L at $x = L$, respectively. The gas contained in the enclosure is assumed to be gray and is considered to absorb, emit, and isotropically scatter the radiation. The surface condition for radiation of the entire enclosure is assumed to be diffuse.

Governing Equations

The Newtonian fluid flow is assumed to be laminar, steady, and two dimensional, and its viscous dissipation is neglected due to its low velocity. Since a very large temperature difference is imposed in this study, the equation of state for ideal gas is used instead of the Boussinesq assumption. The other fluid properties are assumed to be constant as done in Fusegi and Farouk [4]. The governing equations are nondimensionalized using the following variables:

$$x^* = x/L \qquad y^* = y/L \qquad u^* = u/u_o \qquad v^* = v/u_o \tag{1}$$

$$p^* = \frac{p - p_o}{\rho_o u_o^2} \qquad \rho^* = \rho/\rho_o \qquad \mu^* = \mu/\mu_o \qquad k^* = k/k_o \qquad T^* = T/T_o \tag{2}$$

$$\beta_o = \kappa_{ao} + \sigma_{so} \qquad \omega_o = \sigma_{so}/\beta_o \qquad \tau_o = \beta_o L \qquad I^* = \frac{I}{\sigma T_o^4} \tag{3}$$

$$\mathrm{Fr} = \frac{u_o}{\sqrt{gL}} \qquad \mathrm{Pr} = \frac{C_{po}\mu_o}{k_o} \qquad \mathrm{Re} = \frac{\rho_o u_o L}{\mu_o} \qquad \mathrm{Pl} = \frac{k_o/L}{4\sigma T_o^3} \qquad \delta = \frac{T_H - T_C}{T_o} \tag{4}$$

The reference velocity is defined as $u_o = (gL\delta)^{1/2}$ so that Re and Gr are related to be $\mathrm{Re}^2 = \mathrm{Gr}$ [4]. The overheat ratio is denoted by δ. Whereas the reference pressure is atmospheric, the reference temperature is defined as the arithmetic average of the two isothermal wall temperatures, i.e., $T_o = (T_H + T_C)/2$. The reference fluid density is calculated from the ideal equation of state using the gas constant for air, 287 J/(kg · K). The following temperature-dependent transport properties of air at the reference temperature are used:

$$\mu(T) = \frac{14.58 \times 10^{-7} T^{3/2}}{110.4 + T} \ [\mathrm{kg/(m \cdot s)}] \tag{5}$$

$$k(T) = \frac{2.6482 \times 10^{-3} \sqrt{T}}{1 + 245.4 \times 10^{-12/T}/T} \ [\mathrm{W/(m \cdot K)}] \tag{6}$$

$$C_p(T) = 917 + 0.258T - 0.398 \times 10^{-4} T^2 \ [\mathrm{J/(kg \cdot K)}] \tag{7}$$

Based on the presumptions mentioned above, the dimensionless governing equations can be shown as follows:

Continuity equation

$$\frac{\partial}{\partial x^*}(\rho^* u^*) + \frac{\partial}{\partial y^*}(\rho^* v^*) = 0 \tag{8}$$

Momentum equation

$$\frac{\partial}{\partial x^*}(\rho^* u^{*2}) + \frac{\partial}{\partial y^*}(\rho^* u^* v^*) = -\frac{\partial p^*}{\partial x^*} + \frac{1}{\mathrm{Re}}\left[\frac{\partial}{\partial x^*}\left(\mu^* \frac{\partial u^*}{\partial x^*}\right) + \frac{\partial}{\partial y^*}\left(\mu^* \frac{\partial u^*}{\partial y^*}\right)\right] + S_u^*$$

where

$$S_u^* = \frac{1}{\mathrm{Re}}\left[\frac{1}{3}\frac{\partial}{\partial x^*}\left(\mu^* \frac{\partial u^*}{\partial x^*}\right) - \frac{2}{3}\frac{\partial}{\partial x^*}\left(\mu^* \frac{\partial v^*}{\partial y^*}\right) + \frac{\partial}{\partial y^*}\left(\mu^* \frac{\partial v^*}{\partial x^*}\right)\right] \tag{9}$$

$$\frac{\partial}{\partial x^*}(\rho^* u^* v^*) + \frac{\partial}{\partial y^*}(\rho^* v^{*2}) = -\frac{\partial p^*}{\partial y^*} - \frac{1}{\mathrm{Fr}^2}(\rho^* - 1) + \frac{1}{\mathrm{Re}}\left[\frac{\partial}{\partial x^*}\left(\mu^* \frac{\partial v^*}{\partial x^*}\right) + \frac{\partial}{\partial y^*}\left(\mu^* \frac{\partial v^*}{\partial y^*}\right)\right] + S_v^*$$

where

$$S_v^* = \frac{1}{\mathrm{Re}}\left[\frac{1}{3}\frac{\partial}{\partial y^*}\left(\mu^* \frac{\partial v^*}{\partial y^*}\right) - \frac{2}{3}\frac{\partial}{\partial y^*}\left(\mu^* \frac{\partial u^*}{\partial x^*}\right) + \frac{\partial}{\partial x^*}\left(\mu^* \frac{\partial u^*}{\partial y^*}\right)\right] \tag{10}$$

energy equation

$$\frac{\partial}{\partial x^*}(\rho^* u^* T^*) + \frac{\partial}{\partial y^*}(\rho^* v^* T^*) = \frac{1}{\mathrm{Re}\cdot\mathrm{Pr}}\left[\frac{\partial}{\partial x^*}\left(\frac{k^*}{C_p^*}\frac{\partial T^*}{\partial x^*}\right) + \frac{\partial}{\partial y^*}\left(\frac{k^*}{C_p^*}\frac{\partial T^*}{\partial y^*}\right)\right] - \frac{1}{\mathrm{Re}\cdot\mathrm{Pr}}\frac{\tau_o}{\mathrm{Pl}}(1-\omega_o)\frac{1}{C_p^*}\left(T^{*4} - \frac{1}{4}\int_{4\pi} I^* d\Omega\right) \tag{11}$$

equation of state

$$\rho^* = \frac{\rho_o u_o^2}{p_o}\frac{p^*}{T^*} + \frac{1}{T^*} \tag{12}$$

radiative transfer equation

$$\frac{1}{\tau_o}\frac{dI^*(\vec{r},\hat{s})}{ds^*} = \frac{(1-\omega_o)}{\pi}T^{*4}(\vec{r}) - I^*(\vec{r},\hat{s}) + \frac{\omega_o}{4\pi}\int_{4\pi} I^*(\vec{r},\hat{s}')\Phi(\hat{s}',\hat{s})\,d\Omega' \tag{13}$$

In Eq. (13) $\Phi(\hat{s}', \hat{s})$ designates the scattering phase function for radiation from the incoming direction to the outgoing direction. Afterward, the superscript asterisk is dropped for convenience.

Boundary Conditions

The boundary conditions for diffusely reflecting and emitting isothermal opaque walls are as follows:

$$u = v = 0 \qquad T = 1 + \delta/2 \qquad \text{at hot wall at } x = L \tag{14}$$

$$u = v = 0 \qquad T = 1 - \delta/2 \qquad \text{at cold wall at } x = 0 \tag{15}$$

$$I(\vec{r}_w, \hat{s}) = \frac{\varepsilon_w(\vec{r}_w) T^4(\vec{r}_w)}{\pi} + \frac{1 - \varepsilon_w(\vec{r}_w)}{\pi} H(\vec{r}_w) \qquad \text{at ceiling and floor}$$

where

$$H(\vec{r}_w) = \int_{\hat{S}' \cdot \hat{n}_w < 0} I(\vec{r}_w, \hat{s}') \mid \hat{s}' \cdot \hat{n}_w \mid d\Omega' \tag{16}$$

Here, $\varepsilon_w(\vec{r}_w)$ and $\hat{n}_w$ denote the wall emissivity and surface unit normal vector, respectively. $H(\vec{r}_w)$ represents the integration of all incoming directional intensities, i.e., the irradiation. The thermal boundary condition at adiabatic ceiling and floor is found from the following energy balancing equation, in which the net radiation into the wall surface is balanced by conductive heat loss from the wall [10]:

$$\vec{q}^T \cdot \hat{n}_w = -k \nabla T \cdot \hat{n}_w + \frac{\varepsilon_w(\vec{r}_w)}{4\mathrm{Pl}} \left[T^4(\vec{r}_w) - H(\vec{r}_w) \right] = 0 \tag{17}$$

Heat Transfer Rates

To estimate the heat transfer rate at two isothermal walls, various types of average Nu are defined as follows:

$$\overline{\mathrm{Nu}}_w^C = \frac{1}{\delta} \int_0^1 q_w^C dy \tag{18}$$

$$\overline{\mathrm{Nu}}_w^R = \frac{1}{4\mathrm{Pl}\,\delta} \int_0^1 \mathrm{sign}\,(\hat{n}_w) \cdot q_w^R dy \tag{19}$$

$$\overline{\mathrm{Nu}}_w^T = \overline{\mathrm{Nu}}_w^C + \overline{\mathrm{Nu}}_w^R \qquad \text{where } q_w^C = -k \left. \frac{\partial T}{\partial x} \right|_w, \; q_w^R = \int_{4\pi} I(\hat{s}, \hat{n}_w) d\Omega \tag{20}$$

From the above equations, $\overline{\mathrm{Nu}}_w^C$ and $\overline{\mathrm{Nu}}_w^R$ represent the conductive and radiative average Nu's, respectively. Their sum, $\overline{\mathrm{Nu}}_w^T$, is the total average Nu, which denotes the total amount of heat transfer at the wall. Since the steady state is assumed in this study, the total average Nu's at both hot and cold walls would be the same.

NUMERICAL ANALYSIS

Treatment of Adiabatic Baffle

In numerically handling the adiabatic baffles located in the enclosure in Figure 1, it would be inefficient to introduce the curvilinear coordinate system that is aligned to the baffle shape. To overcome this, the rectangular coordinate system is adopted while the whole computational domain including baffles is simultaneously solved by initially assigning the preconditioned values to the nodal points for the adiabatic baffles.

For a typical grid layout shown in Figure 2 *a*, a general form of the discretized equation governing the flow field can be represented by

$$a_P \phi_P = \sum a_{nb} \phi_{nb} + b \tag{21}$$

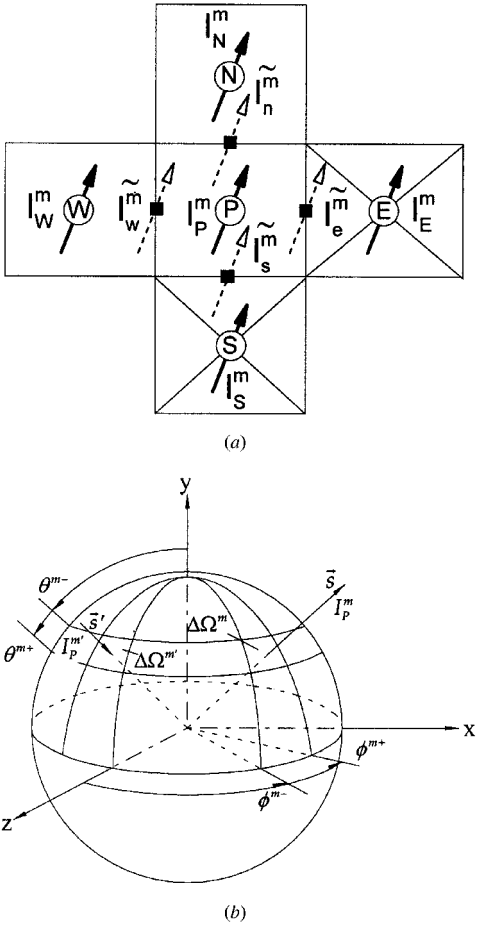

Figure 2. Representation of the spatial control volume and control angle: (*a*) grid layout and typical radiation direction; (*b*) angular discretization used.

To assign an appropriate value to each variable at a node, the additional source term, $\tilde{S} = S_C + S_P\phi_P$ is introduced into the above discretized equation to become

$$(a_P - S_P)\phi_P = \sum a_{nb}\phi_{nb} + b + S_C \tag{22}$$

By setting

$$S_C = M\phi_{\text{fix}} \qquad S_P = -M \tag{23}$$

with a very large number M and substituting it into Eq. (22), it becomes

$$S_C + S_P\phi_P \approx 0 \qquad \text{and then } \phi_P \approx -S_C/S_P \approx \phi_{\text{fix}} \tag{24}$$

since a_P and a_{nb} are all negligible compared with M.

Unfortunately, this simple procedure inherently has major defects due to its artificially introduced large number, so that careful attention is needed to establish a convergence criterion. Furthermore, it would be very difficult to determine an appropriate relaxation factor when the underrelaxation technique is used to promote the convergence. The procedure mentioned above is also hard to employ when the wall function for turbulence, which requires a modification of the source terms near the wall node, is involved in computation. In this study it was found that there was a bit of difficulty in getting a converging solution for the adiabatic wall condition with radiation effects when the computation is iterated. Hence, in this study, instead of introducing an artificial source term, the method that directly adjusts the coefficients relevant to the discretized equations is used. In other words, to assign the value ϕ_{fix} to the internal nodes for the baffle, the coefficients of the relevant discretized equation pertaining to the baffle are set such that

$$a_P = 1 \qquad a_{nb} = 0 \qquad b = \phi_{\text{fix}} \tag{25}$$

Here, ϕ_{fix} is taken to be zero for the computation of velocity while it is the updated temperature for the computation of temperature for the nodes within the baffle. It is also necessary to correct the pressure correction equation to exactly derive the velocity of zero at the baffle zone.

Regarding the radiation, the treatment of the baffle is somewhat different from the previous procedure. The reason is that a control-volume surface intensity is evaluated from the nodal point value using a spatial difference scheme when using the FVM. In other words, while the intensity at the nodal point inside the baffle region must be zero, the intensity at the control-volume surface, which is assumed to be the opaque surface of a baffle, is not zero. Consequently, different from the procedure used for the calculation of the velocity, an adjustment of the coefficients in the relevant discretized equation for radiation is not enough to deal with the baffle. To overcome these difficulties, the additional intensities are introduced at control-volume surfaces as follows.

Using the step scheme [9], the discretized equation for radiation can be expressed by

$$a_P^m I_P^m = a_E^m I_E^m + a_W^m I_W^m + a_N^m I_N^m + a_S^m I_S^m + b^m \tag{26}$$

By introducing the additional control-face intensities, the above equation becomes

$$a_P^m I_P^m = a_E^m \left(I_E^m + \tilde{I}_e^m \right) + a_W^m \left(I_W^m + \tilde{I}_W^m \right) + a_N^m \left(I_N^m + \tilde{I}_n^m \right) + a_S^m \left(I_S^m + \tilde{I}_s^m \right) + b^m \tag{27}$$

where the subscripts e, w, n, s denote the local position of each control face, respectively. Then each nodal point is treated as follows:

$$\tilde{I}_e^m = \tilde{I}_w^m = \tilde{I}_n^m = \tilde{I}_s^m \qquad \text{for usual nodal points} \tag{28}$$

$$a_E^m = a_W^m = a_N^m = a_S^m = b^m = 0 \qquad \text{for nodal points inside the baffle} \tag{29}$$

Besides, handling the nodal points adjacent to the baffle is very clear. For instance, in the case where the east as well as south control face is in contact with the baffle as shown in Figure 2*a*, the $\tilde{I}_s^m$ is calculated from Eq. (16) since it originates from the baffle surface. On the other hand, the $\tilde{I}_e^m$ is found by using the step scheme, since it is the intensity toward the baffle surface. Consequently, it becomes that

$$I_E^m = I_S^m = \tilde{I}_w^m = \tilde{I}_n^m = 0 \qquad \tilde{I}_e^m \neq \tilde{I}_s^m \neq I_W^m \neq I_N^m \neq 0 \tag{30}$$

Because of the inherent nature of the radiation, the intensity at a nodal point is numerically updated following the ray direction. Therefore, additional memory is not required in computation, if the location of the baffle is determined in the process of iteration and the intensity at a control face next to the baffle is estimated. This computational manipulation would be easily extended for the generalized coordinate system.

Computational Procedure

A numerical analysis of thermofluid dynamics characteristics is conducted by adopting the compressible SIMPLER algorithm developed by Karki and Patankar [11]. While the convection term is discretized using the QUICK finite-difference scheme [12], the central difference method is chosen for the diffusion term. To compute the radiation source term in the energy equation, the dimensionless linearized radiative transfer equation is used here as proposed by Chai et al. [9]. A control-volume surface intensity is evaluated from the nodal point value using a step spatial difference scheme [9] to ensure the positive intensity. After some preliminary calculations for checking convergence and accuracy, the spatial and angular domains are discretized into 62×62 nonuniform control volumes in the x and y directions and 2×24 control angles with uniform $\Delta\phi$ and $\Delta\theta$ in ϕ and θ directions, respectively. The typical spatial and angular control volumes are presented in Figure 2.

Computations are proceeded by the following procedures. To begin with, the radiative wall heat fluxes and the source terms in the energy equation are

determined by solving the radiative transfer equation. Then the velocity field is estimated from the momentum equation. After the updated temperature is estimated from the energy equation based on the interior point temperature at the previous iteration, the wall conductive heat fluxes are estimated. Then this information regarding the wall conductive heat flux, the irradiation, and the surface temperature is used to update the nonprescribed wall surface temperatures by solving the energy balance equation (17) with the bisection method. Finally, the convergence criteria are checked if the steady state is reached. Computations are terminated when the difference in total average Nu's for the hot and cold walls is within less than 3% of the total average Nu at the heated wall.

In computation, to reduce the error in the wall conductive heat flux, the grid system should be clustered near the wall; especially near the baffles. Since the calculation of radiative heat fluxes is not necessarily required at every iteration to produce a reliable steady-state result, the radiative heat flux is updated every 10 iterations. However, the wall surface temperature is recalculated and changed at each iteration with an estimated wall conductive heat flux.

Validation of Numerical Results

To validate the present numerical method for pure radiation, test results for a square cavity of 1m × 1m with baffles are compared with those obtained by Coelho et al. [13]. In this problem, one 0.4 m long opaque baffle is centered at a ceiling and two on a floor, 0.2 m apart from the centerline as shown in Figure 3. The emissive power and the absorption coefficient of the medium are 10 W/m^2 and 0.1 m^{-1}, respectively. While the emissivity of the wall is 0.8, that of the baffle is 0.6. An emissive power of unity is assumed for all the walls. While the zero thickness of the baffle is assumed by Coelho et al. [13], here two uniform control volumes are assigned to simulate the baffle. The current results are shown to be in reasonably good agreement with the data obtained by the zone method. It seems that the baffle with finite thickness causes a slight inconsistency in Figure 3, compared with that with zero thickness as adopted by Coelho et al. [13]. When a smaller-sized mesh was used, the results showed better agreement. Consequently, it is concluded that the present numerical method for radiation is good enough to handle a problem with baffles, if more meshes are clustered near the baffle.

The case of natural convection with surface radiation only is also considered for verification by comparison with the experimental results by Bajorek and Lloyd [8]. A square cavity with a length $H = 6.35$ cm, of which upper and bottom walls are thermally insulated, is chosen. Two baffles with $0.1\ H \times 0.25\ H$ each are located at the center of the upper and lower walls. The hot and cold wall temperatures are 312.1 K and 296.6 K, respectively, as it was in the experiment by Bajorek and Lloyd [8]. The medium is air, which is transparent to radiation, so that only surface radiation is involved here. The thermophysical properties are estimated using Eqs. (5)–(7), with respect to the mean medium temperature. The spatial and angular domain consists of 51 × 61 uniform control volumes in the x and y directions and 2 × 24 uniform control angles in the θ and ϕ directions.

The nondimensionalized temperature distribution at the midheight of the cavity is presented in Figure 4. The present results agree very well with the experimental data. The results with radiation effects are in good agreement with

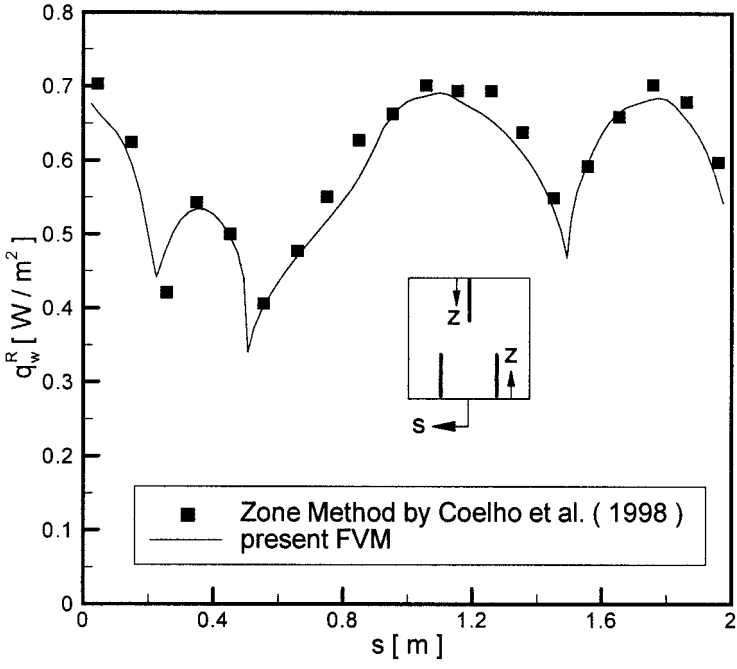

Figure 3. Predicted net radiative heat flux along the boundary of the enclosure.

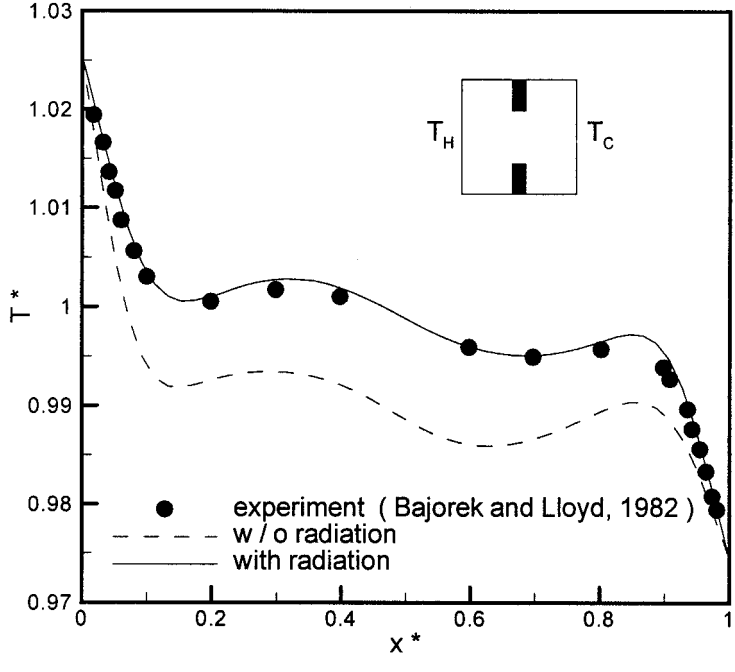

Figure 4. Comparison of experimental results by Bajorek and Lloyd (1982) with temperature distribution calculated along the midheight of the cavity.

the experimental ones. Hence, despite a small temperature difference applied, it is found that the radiation effect cannot be neglected. Based on these validations, the present numerical method is applied to analyzing the natural convection combined with gas and surface radiation in the enclosure in the following.

RESULTS AND DISCUSSION

To discuss the effect of gas and surface radiation on the internal thermofluid field in the rectangular enclosure with baffles, the cold and hot wall temperatures are held at $T_c = 300\ K$ and $T_H = 900\ K$ with overheat ratio of unity. The thermophysical properties are estimated at the reference temperature of 600 K and its corresponding reference Pr becomes 0.684. The Gr is held at 10^5 so that same buoyancy effect is assumed. Two types of baffle configuration are selected as illustrated in Figure 1 and named cases I and II.

In Figures 5 and 6, the effects of radiation on the fluid dynamic and thermal fields are displayed for cases I and II. Each figure is comprised of three conditions,

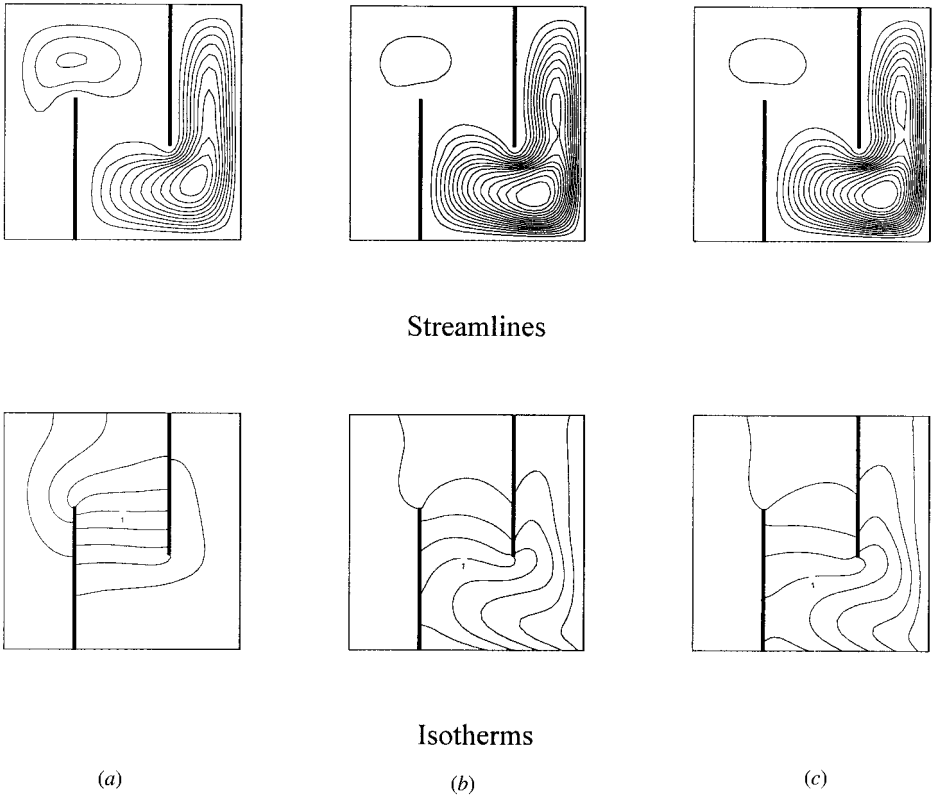

Figure 5. Effects of radiation on streamlines and isotherms for case I: (*a*) pure natural convection only; (*b*) natural convection with surface radiation; (*c*) natural convection with surface and gas radiation, $\tau_o = 1$.

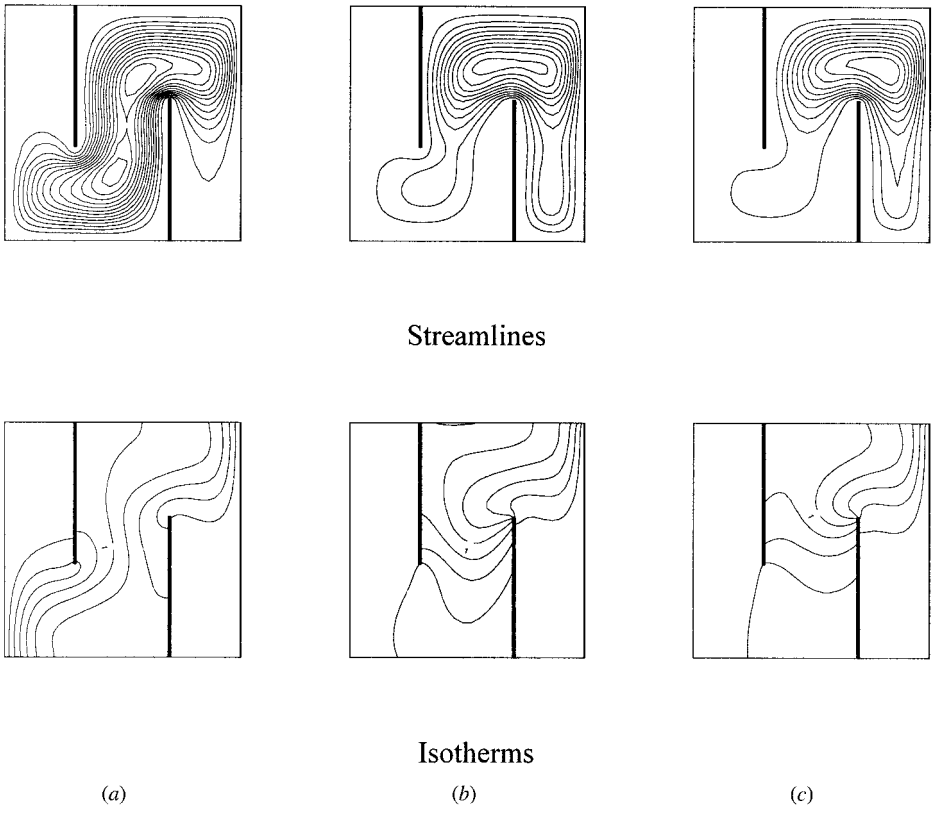

Figure 6. Effects of radiation on streamlines and isotherms for case II: (*a*) pure natural convection only; (*b*) natural convection with surface radiation; (*c*) natural convection with surface and gas radiation, $\tau_o = 1$.

each of which corresponds to the pure natural convection without radiation, natural convection with surface radiation only, and natural convection with surface and gas radiation, respectively. For the case with gas radiation, the radiatively active medium in the enclosure is assumed to be nonscattering, $\omega_o = 0$, with a constant Planck number, Pl = 0.05 and a constant optical thickness, $\tau_o = 1$. All walls including the baffles are assumed to be black. According to the dimensional analysis, the Pl represents the relative importance of the radiation with respect to the conduction so that a decrease in Pl would result in a steeper temperature gradient at the wall. For a participating medium, the radiation source term in the energy equation would play a more significant role as Pl decreases, which leads to more transformation of radiant energy into thermal energy.

When only the pure convection is considered without radiation, the isotherms for case I are seen to be stratified as typically shown in Figure 5*a*. This is because the fluid flow is separated by two incomplete partitions and is contained in two individual convection cells. On the other hand, for case II in Figure 6*a* the hot flow on the left-hand side is seen to penetrate into a region on the right-hand side

through the midzone. It is also noted that the gas or surface radiation does not influence the fluid flow for case I in Figure 5, while it increases the penetration distance for case II in Figure 6. By comparing the isotherms in Figures 5 and 6, the gas or surface radiation is seen to make the temperature more uniform at the region on the left-hand side. Furthermore, the cold region on the right-hand side is more affected by radiation for the geometry for case I, so that a high temperature gradient is developed when the radiation is taken into account, which in turn results in a higher fluid flow as seen in streamlines. It is also noted that the surface radiation is more dominant than the gas radiation. This is inferred from the fact that the results obtained by an addition of gas radiation do not make a noticeable difference.

To explore the heat transfer characteristics for the gas radiation involved at the steady state, a variation of the average Nu with the optical thickness τ_o of the medium is depicted in Figure 7 for cases I and II with Pl = 0.05, $\omega_o = 0$, and black walls. Subscripts L and R indicate the left- and right-hand-side isothermal walls, respectively. The variation of the average Nu because of radiation, $\overline{\mathrm{Nu}}^R$ shows a similar trend in its magnitude for both cases I and II regardless of the optical thickness. Therefore, the orientation of the partitions does not seem to affect the radiative heat flux at both walls. In the figure it is seen that except for a very high optical thickness, $\overline{\mathrm{Nu}}^R$ is much higher than $\overline{\mathrm{Nu}}^C$, so that the radiation is predominant at the left-hand hot wall. However, due to the effect of radiation blockage by partitions, the convection heat transfer at the right-hand cold wall surpasses the radiative heat transfer when the optical thickness is larger than 0.6.

In general, as the optical thickness increases, more radiation is attenuated by the radiative medium. Therefore, as illustrated in Figure 7, for a large optical thickness $\tau_o = 50$, the radiative heat transfer at the right-hand wall becomes small enough to be neglected. The average Nu due to radiation at the left-hand wall, $\overline{\mathrm{Nu}}_L^R$ is also getting smaller so that the average Nu due to convection, $\overline{\mathrm{Nu}}_L^C$ becomes larger therein. Consequently, the total average Nu is shown to decrease as the optical thickness increases. This seems to contradict to the result by Lauriat [2], who solved a simple enclosure problem by introducing the conduction to radiation parameter, $N = k_o \beta_o / (4\sigma T_o^3)$, rather than the Pl, $k_o / (4\sigma T_o^3 L)$. Therefore, the energy balance at an adiabatic wall becomes dependent on the optical thickness τ_o as well as N. That is why the total average Nu increases with increasing τ_o in Lauriat [2]. Hence, it is suggested that the Pl be used as a governing parameter rather than the conduction to radiation parameter, N.

In Figures 8 and 9, the effects of Pl on the flow and thermal fields are represented for $\tau_o = 1$, $\omega_o = 0$ with black walls. Physically, a decrease in Pl results in an increase in the source term in the energy equation (11) so that more radiant energy is absorbed and transformed into thermal energy. Accordingly, the medium temperature in the enclosure is shown to be higher for lower Pl for both cases I and II, as shown in Figures 8 and 9. For case I with Pl = 0.05 (Figure 8*a*), a very steep temperature gradient is formed at the region on the right-hand side so that the fluid flow becomes intense. The total average Nu for Pl = 0.05 is calculated and found to be seven times larger than that for pure convection, Pl = ∞ (Figure 8*d*). For case II in Figure 9, as Pl decreases, the medium temperature at the midsection increases so that the convection cell center migrates toward the upper

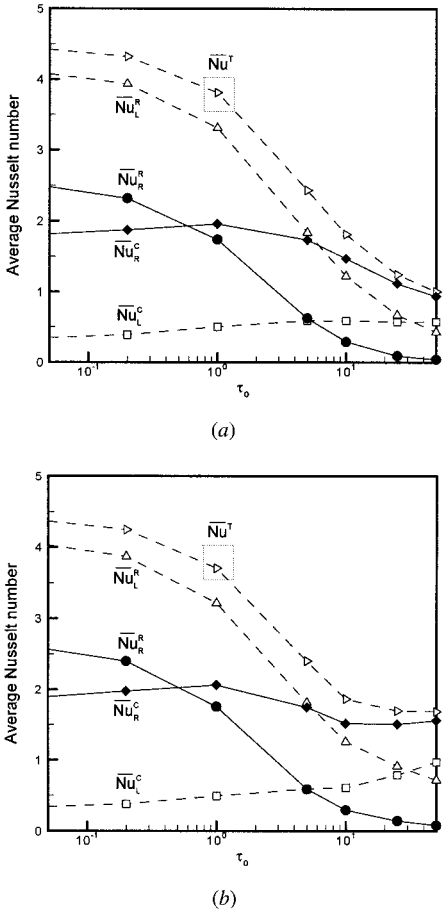

Figure 7. Average Nu's depending on the variations of τ_o with Pl = 0.05, $\omega_o = 0$, and all black walls: (*a*) case I; (*b*) case II.

right. In this type of partition configuration, the total average Nu for Pl = 0.05 is about 2.35 times larger than that for Pl = ∞ (Figure 9*d*). However, the total average Nu's for cases I and II are nearly the same for Pl = 0.05. Otherwise, without radiation, the convective heat transfer from the hot wall to the cold wall for the configuration for case II is three times larger than that for case I. Therefore, as the Pl decreases, the radiation makes up for the difference in the total heat transfer.

Figures 10 and 11 illustrate the effects of the hot and cold wall emissivites, ε_L and ε_R, on the thermofluid behavior for $\tau_o = 0.2$, Pl = 0.05, and $\omega_o = 0$. The adiabatic baffles, ceiling, and floor are all assumed to have black walls. Figures 10*a* and 11*a* are for the case of $\varepsilon_L = \varepsilon_R = 1.0$, i.e., black hot and cold walls. When ε_R becomes zero, i.e., a pure scattering wall, the results are shown in Figures 10*b* and 11*b*. Since radiation cannot be absorbed by the cold and pure scattering wall, a steeper temperature gradient is seen to be developed near the cold wall. In Figure 10*b* for case I, a change in the flow field seems to be minor. However, in Figure 11*b* for case II, because of a higher density gradient near the cold wall, the local fluid flow becomes stronger therein and the convection cell center is seen to

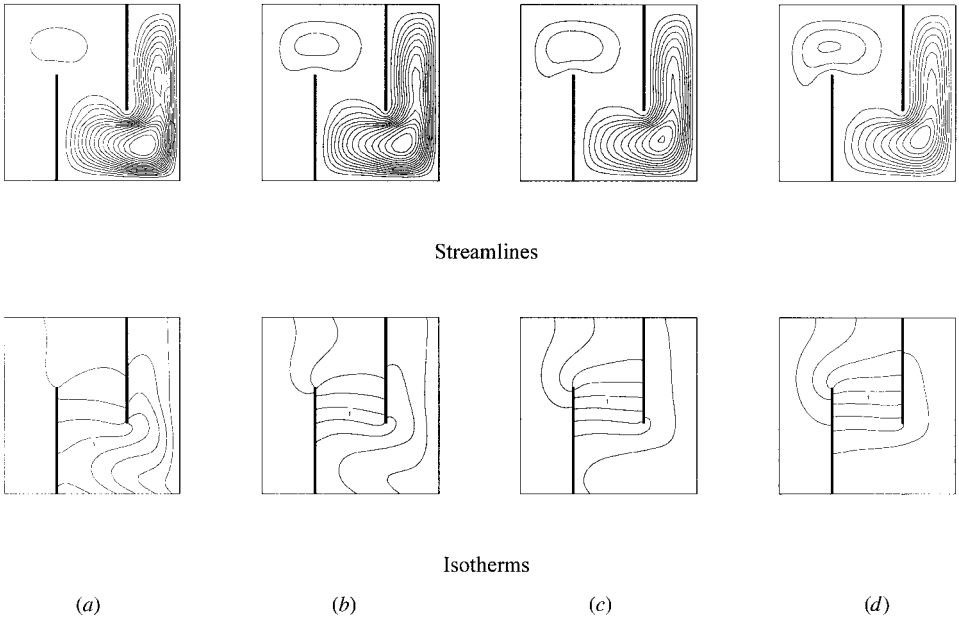

Figure 8. Effects of Pl on the flow and thermal fields for case I with $\tau_o = 1$, $\omega_o = 0$, and black walls: (*a*) Pl = 0.05; (*b*) Pl = 0.2; (*c*) Pl = 1; (*d*) Pl = ∞.

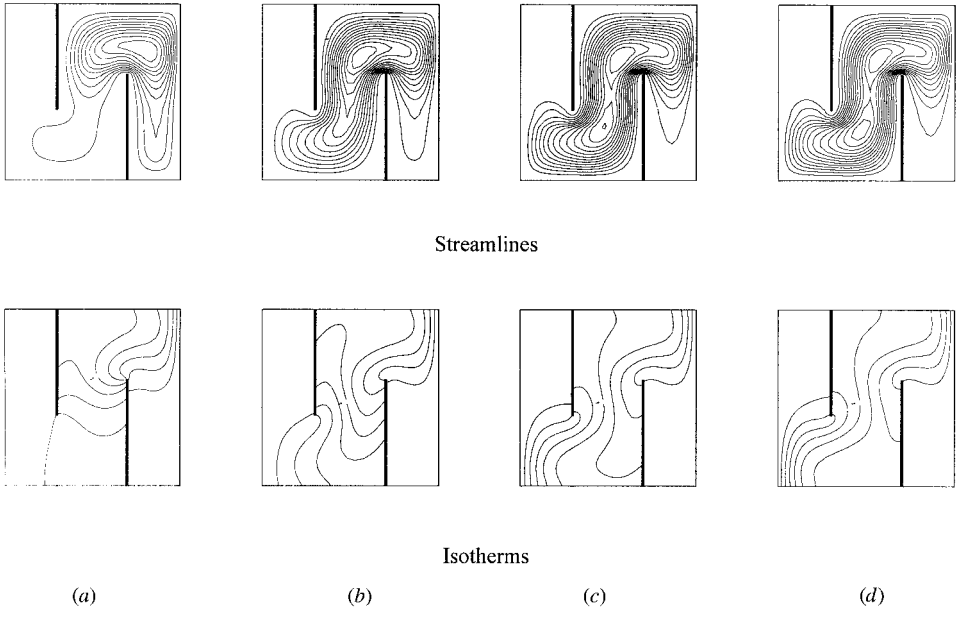

Figure 9. Effects of Pl on the flow and thermal fields for case II with $\tau_o = 1$, $\omega_o = 0$, and black walls: (*a*) Pl = 0.05; (*b*) Pl = 0.2; (*c*) Pl = 1; (*d*) Pl = ∞.

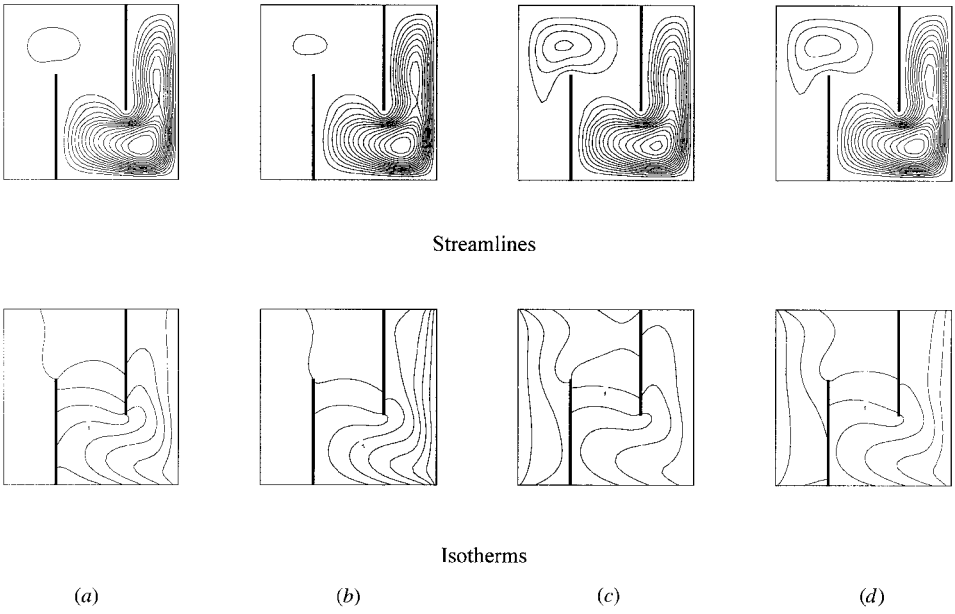

Figure 10. Effects of the isothermal wall emissivities on the flow and thermal fields for case I with $\tau_o = 0.2$, Pl = 0.05, $\omega_o = 0$, and black walls except for isothermal walls: (*a*) all black walls; (*b*) $\varepsilon_L = 1$, $\varepsilon_R = 0$; (*c*) $\varepsilon_L = 0$, $\varepsilon_R = 1$; (*d*) $\varepsilon_L = 0$, $\varepsilon_R = 0$.

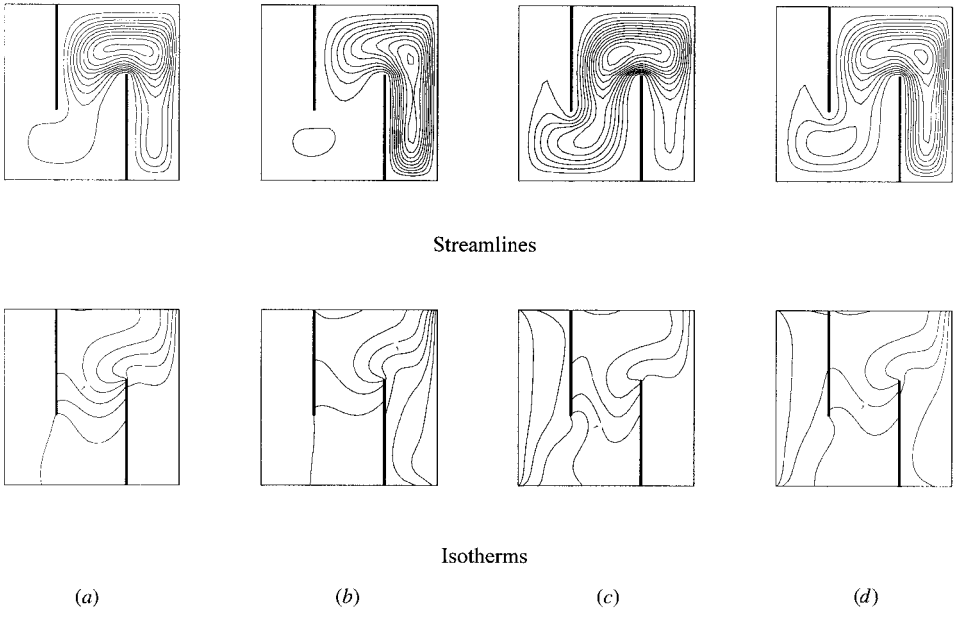

Figure 11. Effects of the isothermal wall emissivities on the flow and thermal fields for case II with $\tau_o = 0.2$, Pl = 0.05, $\omega_o = 0$, and black walls except for isothermal walls: (*a*) all black walls; (*b*) $\varepsilon_L = 1$, $\varepsilon_R = 0$; (*c*) $\varepsilon_L = 0$, $\varepsilon_R = 1$; (*d*) $\varepsilon_L = 0$, $\varepsilon_R = 0$.

migrate toward the cold wall. It is also found that the total average Nu becomes lower, since there is no radiative absorption at the cold wall.

When the hot wall emissivity is zero and the cold wall emissivity is unity, a steeper temperature gradient is now developing near the hot wall as shown in Figures 10*c* and 11*c*. Since a density gradient is evolving near the hot wall, the stronger convection cell is formed at the upper-left corner for case I (Figure 10*c*), whereas the main flow is being extended to the lower-left corner for case II (Figure 11*c*). The average Nu for the black hot wall is found to be about 1.5 times bigger than that for the black cold wall when the other wall emissivity is zero. Finally, when the hot and cold walls are all zero, the temperature gradient becomes steep at both wall as in Figures 10*d* and 11*d* and the effects of the radiative transfer are reduced.

The effects of the scattering albedo are illustrated in Figures 12 and 13 for $\tau_o = 1$, Pl = 0.05, and black walls. Here, only the isotropic scattering is considered. As can be seen in the figures, the effects of the scattering on the thermal and flow field are negligible, even for the pure scattering, $\omega_o = 1$, so that the variation in the average Nu is also found to be within a few percent.

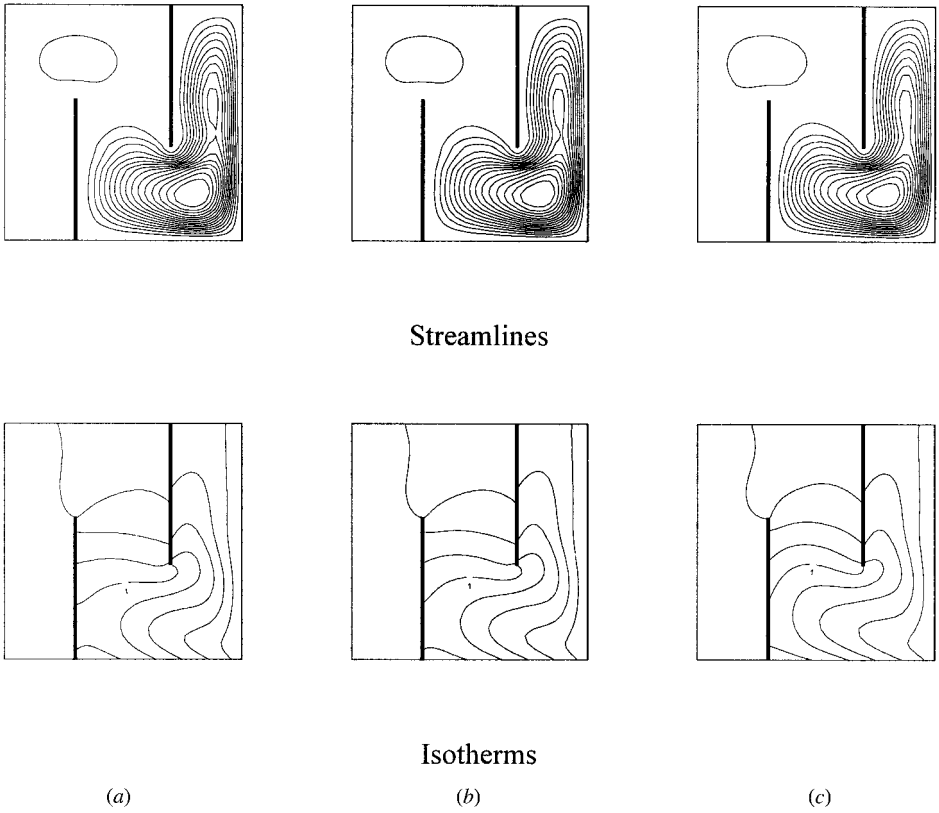

Figure 12. Effects of the scattering albedo on the fluid dynamics and thermal fields for case I with $\tau_o = 1$, Pl = 0.05, and black walls: (*a*) $\omega_o = 0.1$; (*b*) $\omega_o = 0.5$; (*c*) $\omega_o = 1$.

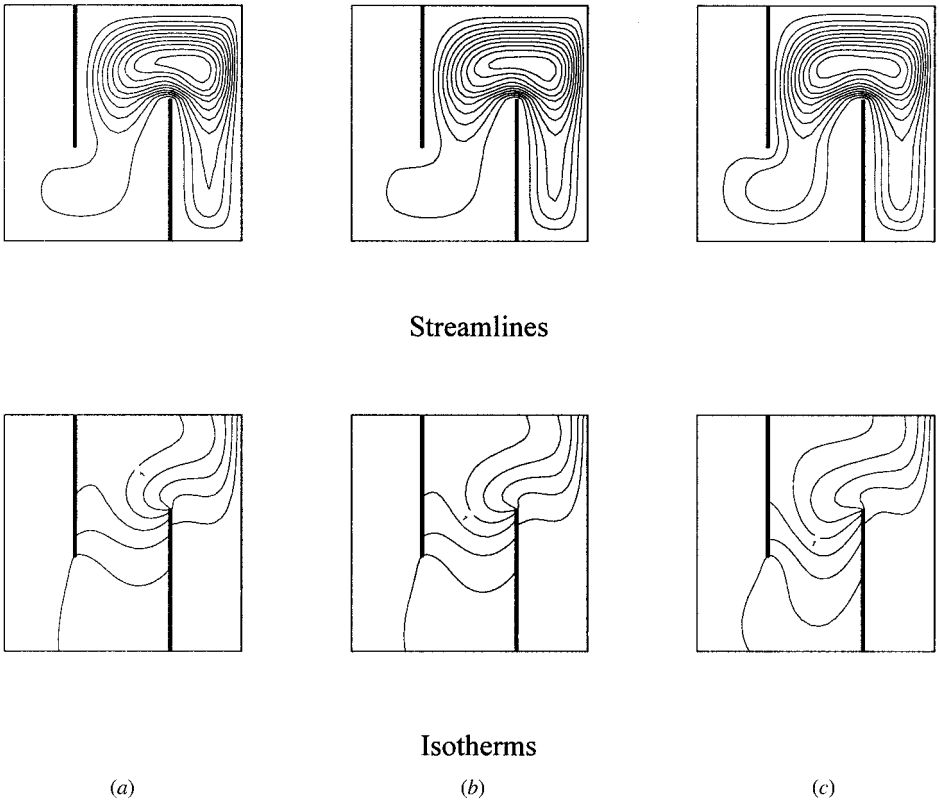

Figure 13. Effects of the scattering albedo on the fluid dynamics and thermal fields for case II with $\tau_o = 1$, Pl = 0.05, and black walls: (*a*) $\omega_o = 0.1$; (*b*) $\omega_o = 0.5$; (*c*) $\omega_o = 1$.

The effects of the emissivity of baffles are presented in Figures 14 and 15 for $\tau_o = 0.2$, Pl = 0.05, and $\omega_o = 0$ with black walls. When the emissivity of baffles is zero, the baffles act as adiabatic walls only for conduction so that the isotherms are seen to be normal to the baffles as in Figures 14*a* and 15*a*. But for emissivity of 1, the isotherms are not normal to the baffles since they are adibatic for the radiation as well as for the conduction. It is also seen that the effects of the baffle emissivity on the thermofluid behavior are more apparent for the baffle configuration for case II.

CONCLUSIONS

A numerical investigation has been performed to examine the radiation-affected steady-laminar natural convection in the enclosure when two incomplete partitions exist. Two different baffle configurations were considered. The radiation exerted a noticeable influence on the fluid dynamic and thermal fields compared

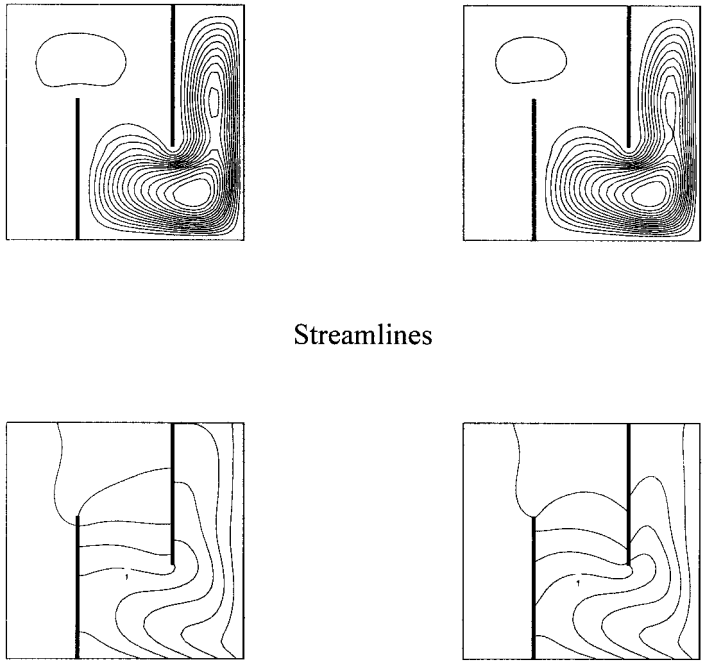

Figure 14. Effects of the emissivity of baffles on the fluid dynamics and thermal fields for case I with $\tau_o = 0.2$, Pl = 0.05, $\omega_o = 0$, and black walls except for the baffles: (*a*) $\varepsilon_{\text{baffle}} = 0$; (*b*) $\varepsilon_{\text{baffle}} = 1$.

with ones without radiation. But the surface radiation played a more important role than the gas radiation. Depending on the baffle configuration, there was a difference in the effects of radiation. The main results are as follows:

(1) When the pure convection is considered, the isotherms are stratified for case I, because the fluid is trapped between two incomplete partitions. Two convection cells are separated. For case II, two convection cells merged.
(2) With radiation, the temperature at the region near the hot wall is more uniform and the region near the cold wall is more thermally affected.
(3) Except for the very high optical thickness, the radiation is a main heat transfer mode near the hot wall. However, because of the radiation blockage by partitions, the convective heat transfer surpasses the radiative heat transfer at the cold wall on the right-hand side for optical

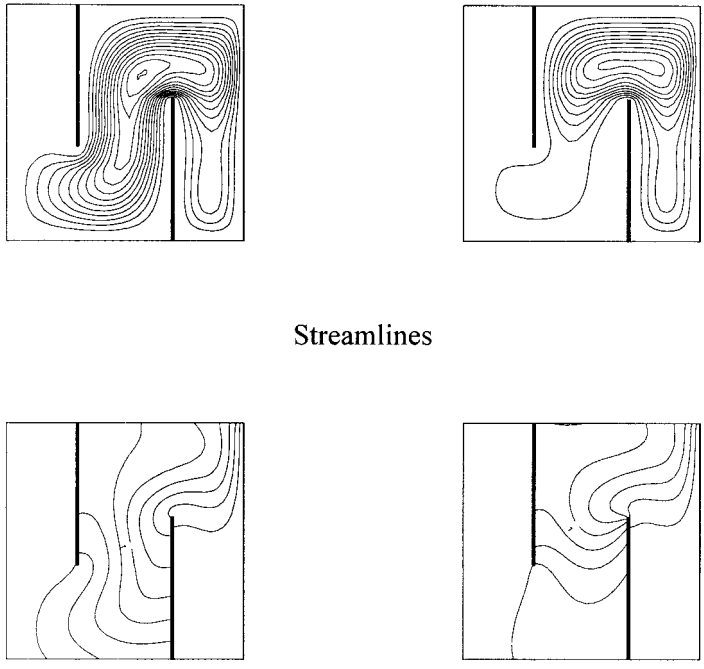

Figure 15. Effects of the emissivity of baffles on the fluid dynamics and thermal fields for case II with $\tau_o = 0.2$, Pl = 0.05, $\omega_o = 0$, and black walls except for the baffles: (*a*) $\varepsilon_{\text{baffle}} = 0$; (*b*) $\varepsilon_{\text{baffle}} = 1$.

thickness larger than 0.6. The total average Nu is also found to decrease as the optical thickness increases.

(4) The effect of radiation cannot be neglected if the Pl is less than unity. For case I, as Pl increases, the temperature gradient near the hot wall becomes more apparent so that the local convection on the upper-left corner intensified. For case II, as the Pl decreases, the medium temperature increases so that the convection cell center moves to the upper-right corner.

(5) The variation in the emissivity of the isothermal walls as well as the baffles results in the distinct changes in the thermal and flow fields, depending on the baffle configuration. However, no apparent changes in the thermal and flow fields occur with the isotropic scattering albedo, because the scattering albedo hardly affects the thermal boundary condition for the adiabatic wall.

REFERENCES

1. N. C. Markatos and K. A. Pericleous, Laminar and Turbulent Natural Convection in an Enclosed Cavity, *International Journal of Heat and Mass Transfer*, vol. 27, no. 5, pp. 755–772, 1984.
2. G. Lauriat, Combined Radiation-Convection in Gray Fluids Enclosed in Vertical Cavities, *Journal of Heat Transfer*, vol. 104, pp. 609–615, 1982.
3. A. Yucel, S. Acharya, and M. L. Williams, Natural Convection and Radiation in a Square Enclosure, *Numerical Heat Transfer*, *Part A*, vol. 15, pp. 261–278, 1989.
4. T. Fusegi and B. Farouk, Laminar and Turbulent Natural Convection-Radiation Interactions in a Square Enclosure Filled with a Nongray Gas, *Numerical Heat Transfer*, *Part A*, vol. 15, pp. 303–322, 1989.
5. M. W. Nansteel and R. Greif, Natural Convection in Undivided and Partially Divided Rectangular Enclosures, *Journal of Heat Transfer*, vol. 103, pp. 623–629, 1981.
6. N. N. Lin and A. Bejan, Natural Convection in a Partially Divided Enclosure, *International Journal of Heat and Mass Transfer*, vol. 26, no. 12, pp. 1867–1878, 1983.
7. L. C. Chang, K. T. Yang, and J. R. Lloyd, Radiation-Natural Convection Interactions in Two-Dimensional Complex Enclosures, *Journal of Heat Transfer*, vol. 105, pp. 89–95, 1983.
8. S. M. Bajorek and J. R. Lloyd, Experimental Investigation of Natural Convection in Partitioned Enclosures, *Journal of Heat Transfer*, vol. 104, pp. 527–532, 1982.
9. J. C. Chai, H. S. Lee, and S. V. Patankar, Treatment of Irregular Geometries Using a Cartesian Coordinates Finite-Volume Radiation Heat Transfer Procedure, *Numerical Heat Transfer*, *Part B*, vol. 26, pp. 225–235, 1994.
10. E. H. Chui, P. M. J. Hughes, and G. D. Raithby, Implementation of the Finite Volume Method for Calculating Radiative Transfer in a Pulverized Fuel Flame, *Combustion Science and Technology*, vol. 92, pp. 225–242, 1993.
11. K. C. Karki and S. V. Patankar, Pressure Based Calculation Procedure for Viscous Flows at All Speeds in Arbitrary Configurations, *AIAA Journal*, vol. 27, no. 9, pp. 1167–1174, 1989.
12. S. Thakur and W. Shyy, Some Implementational Issues of Convection Schemes for Finite-Volume Formulations, *Numerical Heat Transfer*, *Part B*, vol. 24, pp. 31–55, 1993.
13. P. J. Coelho, J. M. Goncalves, and M. G. Carvalho, Modelling of Radiative Heat Transfer in Enclosures with Obstacles, *International Journal of Heat and Mass Transfer*, vol. 41, nos. 4–5, pp. 745–756, 1998.
14. C. Y. Han, and S. W. Baek, Natural Convection Phenomena Affected by Radiation in Concentric and Eccentric Horizontal Cylindrical Annuli, *Numerical Heat Transfer*, *Part A*, vol. 36, pp. 473–488, 1999.